

# THE SLOAN LENS ACS SURVEY. VIII. THE RELATION BETWEEN ENVIRONMENT AND INTERNAL STRUCTURE OF EARLY-TYPE GALAXIES<sup>1</sup>

TOMMASO TREU<sup>2,3</sup>, RAPHAËL GAVAZZI<sup>2,4</sup>, ALEXIA GORECKI<sup>2</sup>, PHILIP J. MARSHALL<sup>2</sup>, LÉON V. E. KOOPMANS<sup>5</sup>, ADAM S. BOLTON<sup>6</sup>, LEONIDAS A. MOUSTAKAS<sup>7</sup>, AND SCOTT BURLES<sup>8</sup>

*submitted to ApJ*

## ABSTRACT

We study the relation between the internal structure of early-type galaxies and their environment using 70 strong gravitational lenses from the Sloan ACS Lens Survey (SLACS). The Sloan Digital Sky Survey (SDSS) database is used to determine two measures of overdensity of galaxies around each lens: the projected number density of galaxies inside the tenth nearest neighbor ( $\Sigma_{10}$ ) and within a cone of radius one  $h^{-1}$  Mpc ( $D_1$ ). Our main results are: 1) Lenses prefer overdense environments as expected for massive early-type galaxies (12/70 are in groups or clusters). 2) The distribution of overdensities is indistinguishable from that of “twin” non-lens galaxies selected from SDSS to have the same redshift and stellar velocity dispersion  $\sigma_*$ . Thus, within our errors, lens galaxies are an unbiased population, and the SLACS results can be generalized to the overall population of early-type galaxies. 3) Typical contributions from external mass distribution are no more than a few per cent in local mass density, reaching 10-20% ( $\sim 0.05 - 0.10$  external convergence) only in the most extreme overdensities. 4) No significant correlation between overdensity and slope of the mass density profile of the lens galaxies is found. 5) Satellite galaxies (those with a more luminous companion) have marginally steeper mass density profiles (as quantified by  $f_{\text{SIE}} = \sigma_*/\sigma_{\text{SIE}} = 1.12 \pm 0.05$  vs  $1.01 \pm 0.01$ ) and smaller dynamically normalized mass enclosed within the Einstein radius ( $\Delta \log M_{\text{Ein}}/M_{\text{dim}}$  differs by  $-0.09 \pm 0.03$  dex) than central galaxies (those without). This result suggests that tidal stripping may affect the mass structure of early-type galaxies down to kpc scales probed by strong lensing, when they fall into larger structures.

*Subject headings:* gravitational lensing — galaxies: elliptical and lenticular, cD — galaxies: evolution — galaxies: formation — galaxies: structure

## 1. INTRODUCTION

The observed properties of galaxies correlate with their environment. For example, the mix of morphological types depend on the local number density of galaxies (Dressler 1980a,b; Postman & Geller 1984; Dressler et al. 1997; Treu et al. 2003; Postman et al. 2005; Smith et al. 2005; Capak et al. 2007) and dark matter (Lane et al. 2007), with elliptical galaxies dominating in high density regions. The star-formation rate and colors of galaxies also scale with their local number density, or distance from the center of clusters (e.g.,

Balogh et al. 2004; Goto et al. 2003; Hogg et al. 2004; Cooper et al. 2008).

The physical origin of these environmental trends has been studied for over thirty years. A number of mechanisms have been proposed to shut off or trigger star-formation as well as to modify the mass-dynamical structure of galaxies. They include interactions with other galaxies (mergers or harassment), with the dark-matter potential of clusters and groups (tidal stripping; tidal compression, harassment) and with the intracluster medium when present (starvation or strangulation, ram pressure stripping). A review of the main mechanisms, their effects on galaxies, and the range of environments over which they operate is given by Treu et al. (2003). Although the interaction between galaxies and their environment is not yet fully understood, comprehensive analyses of large imaging and spectroscopic datasets over a range of environments and cosmic times have shown that a variety of mechanisms are at work, starting from the very outskirts of clusters. Physical processes such as starvation and harassment start to be effective at the group stage or when galaxies infall onto clusters as groups, beyond the cluster virial radius. At higher densities other mechanisms such as ram pressure stripping become effective, further modifying the properties of galaxies.

To complement the progress based on traditional luminous tracers of star-formation and morphology, it is clear that one can gain additional insights by following the modifications to the mass-dynamical structure of galaxies induced by the environment. Empirical scaling laws connecting stellar populations with kinematics,

<sup>1</sup> Based on observations made with the NASA/ESA Hubble Space Telescope, obtained at the Space Telescope Science Institute, which is operated by the Association of Universities for Research in Astronomy, Inc., under NASA contract NAS 5-26555. These observations are associated with programs #10174, #10587, #10886, #10494, #10798.

<sup>2</sup> Department of Physics, University of California, Santa Barbara, CA 93106, USA (tt@physics.ucsb.edu, pj@physics.ucsb.edu)

<sup>3</sup> Sloan Fellow; Packard Fellow

<sup>4</sup> Institut d’Astrophysique de Paris, UMR7095 CNRS - Université Paris 6, 98bis Bd Arago, 75014 Paris, France (gavazzi@iap.fr)

<sup>5</sup> Kapteyn Institute, P.O. Box 800, 9700AV Groningen, The Netherlands (koopmans@astro.rug.nl)

<sup>6</sup> Beatrice Watson Parrent Fellow, Institute for Astronomy, University of Hawai’i, 2680 Woodlawn Dr., Honolulu, HI 96822 (bolton@ifa.hawaii.edu)

<sup>7</sup> Jet Propulsion Laboratory, 4800 Oak Grove Dr, Caltech, MS169-327, Pasadena CA 91109 (leonidas@jpl.nasa.gov)

<sup>8</sup> Department of Physics and Kavli Institute for Astrophysics and Space Research, Massachusetts Institute of Technology, 77 Massachusetts Ave., Cambridge, MA 02139, USA (burles@mit.edu)

such as the fundamental plane and the Tully Fisher relation, have suggested mild trends of the star-formation history of early-type galaxies with environment, and that spiral galaxies are dynamically perturbed as they enter massive clusters (e.g. Moran et al. 2007, and references therein).

Gravitational lensing provides an additional tool to address the connection between galaxies and their environment. By measuring total mass directly — rather than through optical tracers — gravitational lensing gives a direct handle on the transformations of the mass dynamical structure. For example, weak galaxy-galaxy lensing studies in clusters have shown that dark-matter halos of infalling galaxies are tidally truncated (Natarajan et al. 2002a; Gavazzi et al. 2004; Natarajan et al. 2007).

In this paper we exploit the large and homogeneous sample of strong gravitational lenses discovered by the Sloan Lenses ACS Survey (Bolton et al. 2006; Treu et al. 2006; Koopmans et al. 2006; Gavazzi et al. 2007; Bolton et al. 2008a; Gavazzi et al. 2008; Bolton et al. 2008b, hereafter collectively SLACS, or SLACS Papers I through VII) to study the connection between environment and mass-dynamical structure at the typical scale of galaxy strong lensing (i.e.  $\sim 10\text{kpc}$ ). At these scales the mass distribution is more directly connected with morphology and stellar populations than at the larger scales probed by weak lensing.

Two main effects are expected. On the one hand we expect that tidal truncation by an external potential could steepen the local mass density slope, as suggested for the case of PG1115+080 (Impey et al. 1998; Treu & Koopmans 2002b), by numerical simulations (Dobke et al. 2007), and by an analysis of the first 15 lenses in the SLACS sample (Auger 2008). If this is the case, then we would expect empirical scaling relations — such as the correlation between velocity dispersion of the best fit lens model and stellar velocity dispersion and the mass plane (MP; Bolton et al. 2007) — to depend on the environment. On the other hand, since lensing only measures projected mass, a high density environment with a relatively smooth and shallow embedding dark-matter halo could mimic a shallower local slope and therefore skew measurements in the opposite direction. One of the goals of this paper is to clarify these issues in order to improve our understanding of the internal structure of lens galaxies, and therefore of early-type galaxies in general if lenses are an unbiased subset.

In addition to providing a diagnostic of the interaction between galaxies and their environment — and of the internal structure of early-type galaxies — this study also has repercussions for a number of applications of gravitational lensing. For example, the degeneracy between local mass density slope and external mass density is the dominant source of error in measuring the Hubble Constant from gravitational time delays (e.g., Kochanek 2002; Koopmans et al. 2003; Moustakas et al. 2007; Oguri 2007; Suyu et al. 2008). Discovering trends with the local environment may help reduce systematic errors in these measurements. Similarly, the effects of the local environment need to be taken into account to interpret weak galaxy-galaxy lensing results, as well as to do precision cosmography based on lensing statistics.

In previous Papers (I,II,IV,V) we showed that the SLACS lenses are statistically indistinguishable within

the current level of measurement errors from control samples in terms of properties such as size, luminosity, surface brightness, location on the Fundamental Plane, and weak lensing signal, and thus our results could be generalized to the overall population of early-type galaxies. In this paper, we address the question of whether the environment of SLACS lens galaxies differs from that of non-lens galaxies with the same properties, using samples of “twin galaxies” (or simply “twins”) selected to have the same stellar velocity dispersion and redshift.

The paper is organized as follows. In Section 2 we briefly review the SLACS sample, describe the selection of a sample of twin galaxies from the Sloan Digital Sky Survey (SDSS), and present our new measurements of local environment. In Section 3 we discuss whether the environments of lens galaxies are special compared to those of non-lens galaxies with similar properties. In Section 4 we explore the dependence of the internal structure of early-type galaxies on the environment. In Section 5 we discuss our findings, and in Section 6 we provide a summary.

Throughout this paper magnitudes are given in the AB scale. We assume a concordance cosmology with matter and dark energy density  $\Omega_m = 0.3$ ,  $\Omega_\Lambda = 0.7$ , and Hubble constant  $H_0 = 100h\text{kms}^{-1}\text{Mpc}^{-1}$ , with  $h = 0.7$  when necessary.

## 2. SAMPLE SELECTION AND DATA ANALYSIS

Section 2.1 summarizes the SLACS selection process, reviews the properties of the SLACS lenses analyzed in this study, and describes the selection of a control sample of “twins” from the Sloan database. Section 2.2 presents our measurements of environment.

### 2.1. SLACS lenses and SDSS twins

The sample analyzed in this paper is composed of the early-type lens galaxies identified by the SLACS Survey. We include all the 70 lenses classified as definite (grade “A”), including 63 successfully modeled as a single singular isothermal ellipsoid. The seven unmodeled lenses (see paper V for details) include three classified as complex, i.e. where a single singular isothermal ellipsoid is not a good description due to the presence of a very close nearby companion. We do not exclude those from the sample not to introduce biases against high density environments. The vast majority of the lenses are morphologically classified (paper V) as early-type galaxies (62/70), a small fraction are classified as disk galaxies (6/70), and 2/70 have ambiguous morphology.

A full description of the SLACS Survey and the selection process — together with images of all the lenses discovered with the Advanced Camera for Surveys (ACS) — is given in papers I and V of this series (Bolton et al. 2006, 2008; see also Bolton et al. 2004, 2005 and the SLACS website at [www.slacs.org](http://www.slacs.org)). For easy reference, we give here a brief summary. First, lens candidates are found in the SDSS database by identifying composite spectra made of a quiescent stellar population and multiple emission lines at a higher redshift. The spectra are taken from the Luminous Red Galaxies sample (Eisenstein et al. 2001) and the MAIN galaxy sample (Strauss et al. 2002). Quiescent spectra are selected from the MAIN sample by imposing a limit on the rest-frame equivalent width of  $H\alpha < 4\text{\AA}$ .

Second, the probability of the candidate being a lens as opposed to a chance overlap within the fiber is computed based on the SDSS stellar velocity dispersion, the lens and source redshifts, and an isothermal mass model. In this model, the probability of being a lens is a monotonically increasing function of Einstein radius and therefore, for any given source and lens redshift, of velocity dispersion. As discussed in Papers II and V, velocity dispersion and redshift appear to be the two most important parameters characterizing the properties of the lenses.

Third, the most promising candidates have been imaged with ACS on board the *Hubble Space Telescope* (HST) to confirm the lens hypothesis (Programs 10174, 10587, 10886). Confirmed lenses are followed-up with ACS and NICMOS to obtain deep three color images (Programs 10494, 10798, 11202). After the failure of ACS, Programs 10886, 10494 and 10798 have been switched to the Wide Field and Planetary Camera 2 (WFPC2). The follow-up programs are still ongoing. The present analysis is based on the ACS dataset described in paper V.

For each lens, the following quantities are available from Paper V: coordinates, redshift of the lens and source, F814W magnitude, rest-frame V-band magnitude, effective radius, axis ratio, position angle, morphology, stellar velocity dispersion, and Einstein radius (as derived from a singular isothermal ellipsoid lens model).

In order to compare the environment of SLACS lenses with those of non-lens galaxies, we randomly select for each SLACS lens a sample of 100 “twins,” i.e. galaxies with virtually the same velocity dispersion and redshift. Note that the SLACS series adopts stellar velocity dispersion measurements based on the specBS pipeline developed by David Schlegel, with cuts in signal-to-noise ratio (see discussion in Bolton et al. 2008a). This estimate is not available for a few of the lens galaxies. Therefore, in order to ensure uniform and self consistent measurements for all lenses, we use the standard stellar velocity dispersion from the SDSS-DR6 database (Adelman-McCarthy et al. 2008) as a matching parameter between lenses and twins.

One hundred twins are found for each lens. Fifty twins are chosen to have velocity dispersion just above that of the lens and the remaining fifty have velocity dispersions just below that of the lens. This ensures an unbiased comparison sample (cf. discussion in papers II and V). The number of twins per lens is sufficiently high to make errors on the average properties of the comparison sample negligible with respect to those on the SLACS lenses. At the same time, one hundred twins are available for every lens and they are a tractable number for quality control, as described in § 2.2.

## 2.2. Environment measures

We measure two standard environment parameters (see, e.g., Cooper et al. 2005) using the SDSS database: i) the projected number density of galaxies inside the circle of radius equal to the projected distance to the tenth nearest neighbor of the lens  $\Sigma_{10}$  (see Dressler 1980b); ii) the projected number density of galaxies within a  $1 h^{-1}$  Mpc radius circle  $D_1$  (i.e. the typical scale of a cluster). For brevity we refer to those two measures of environment as “local” and “global” density. We choose the term local and global to emphasize that  $\Sigma_{10}$  is an adap-

tive measure that can be sensitive to overdensities on small scales, like subclumps or cores of clusters of galaxies, while  $D_1$  is by construction sensitive to overdensities on the typical scale of an entire cluster. Therefore in general we expect the dynamic range of  $\Sigma_{10}$  to be larger than that of  $D_1$ . Both quantities are measured in units of  $\text{Mpc}^{-2}$ .

In practice we proceed as follows. For each lens we query the SDSS database and retrieve a catalog (hereafter “cone”) of all the objects within a one  $h^{-1}$  Mpc radius. In the present analysis we limit ourselves to the photometric catalogs, since spectroscopic catalogs are rather sparse (except for the lowest redshift lenses) and are biased by the fiber positioning strategy of the SDSS. We then select objects belonging to the environment of the lens based on their magnitude and photometric redshifts (Csabai et al. 2003). We adopt the following magnitude limits and redshift intervals:  $i' < i'_{\text{lens}} + 3$ ,  $z_{\text{lens}} + \delta z_{\text{lens}} > z > z_{\text{lens}} - \delta z_{\text{lens}}$ , with  $\delta z_{\text{lens}} = 0.03(1 + z_{\text{lens}})$ . For brevity, galaxies within these magnitude and photo-z intervals are referred to as “neighbors.” The magnitude limit ensures that even the faintest galaxies in our environment samples are brighter than  $i' = 21$ , ensuring accurate photometric redshifts (Csabai et al. 2003), while the redshift range represents a compromise between completeness and purity. In general, photo-z slices much smaller than our choice have to be discarded because they become smaller than photo-z accuracy and comparable with peculiar velocities expected in clusters, while photo-z slices much larger than our choice tend to dilute the signature of the local environment. We have verified that our measurements are robust with respect to reasonable changes of magnitude cuts and photometric redshift slices. In order to prevent biases due to edge effects or gaps in the photo-z catalog (due, e.g., to bright stars) all catalogs are visually inspected. Four of the lenses have incomplete cones, leaving a total sample of sixty-six lenses with reliable environment measures<sup>9</sup>.

We note that the absolute values of  $\Sigma_{10}$  and  $D_1$  depend on the adopted magnitude and redshift limits (e.g. Treu et al. 2003). Therefore, in order to interpret our environment measures we need to consider properly normalized quantities. To this aim, we perform the same measurements around pointings randomly selected from the SDSS archive. The average densities of neighbors measured from one hundred random fields with the appropriate cuts in magnitude and redshift for each lens are referred to as  $\langle \Sigma_{10} \rangle = \langle D_1 \rangle$ . Note that the average density of the Universe is independent of the adopted aperture, so the two quantities are the same when averaged over random pointings. The uncertainty on the mean is also very similar, since a random cone of radius one  $h^{-1}$  Mpc contains approximately 10 galaxies for the typical magnitude and redshift cuts of our survey. Throughout this study we will adopt as environment measures local and global *overdensities* defined as  $\Sigma_{10}/\langle \Sigma_{10} \rangle$  and  $D_1/\langle D_1 \rangle$ . As discussed, e.g., by Hogg et al. (2003) and Cooper et al. (2006) this procedure allows one to compare data of different intrinsic depth. Furthermore, the

<sup>9</sup> For six of the sixty-six lenses there are fewer than 10 neighbors within each cone (at least 7 in any case). In those cases the local density is set equal to the global density. Thus  $D_1 \leq \Sigma_{10}$ , by definition.

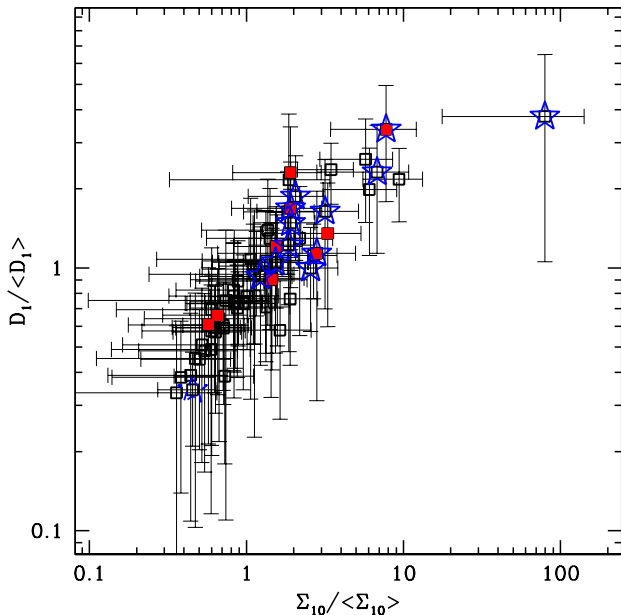


FIG. 1.— Distribution of environment estimators for the SLACS sample. Matches with known groups/clusters are identified by blue open stars. Red solid points identify “satellite” galaxies, as described in the main text. The lens with the highest overdensity (J1143-0144) is known to be part of the optically selected cluster Abell 1364 (Figure 2). The lens associated with a known group/cluster at the lower end of the overdensity range (J0252+0039; identified by a dashed blue star), is associated with cluster candidate NSCSJ025225+003540. Inspection of the field via SDSS multicolor images shows no sign of a cluster near. We thus consider this identification as spurious (see text for details).

distribution of density for the random fields allows us to estimate the uncertainty due to sample variance, photometric redshift uncertainties, and incompleteness. To be conservative, we adopt as errors on the overdensity the sum in quadrature of the Poisson uncertainty on the density measures, and of the sample variance of the random fields as an upper limit to all other uncertainties.

To address the issue of whether the environments of lenses are special, we perform the same measurements for the twins of each lens. After visual inspection to reject a few corrupted catalogs by bright stars or survey edges, we compute  $\Sigma_{10}$  and  $D_1$  for the twins. Table 1 lists for each lens  $\Sigma_{10}$  and  $D_1$ , as well as the average of the same quantities measured for the random fields ( $\langle\Sigma_{10}\rangle = \langle D_1\rangle$ ), and for the twins ( $\langle\Sigma_{10}\rangle_t$  and  $\langle D_1\rangle_t$ ).

In addition, we compute the number of neighbors in each cone significantly brighter (i.e.  $i' < i'_{\text{lens}} - 1$ ) than the lens to determine whether the galaxy is the central galaxy of the “cone” (and thus presumably of the halo associated with the overdensity), or rather a satellite to a larger galaxy. The difference in magnitude is chosen as a compromise to identify significantly more massive companions while preserving enough statistics. Our conclusions are not changed significantly if a threshold of 0.5 or 1.5 magnitudes is adopted instead.

We define as “satellite” galaxies those with at least one neighbor brighter than the lens galaxy by at least one magnitude, and “central” galaxies all the others. In the remainder of this paper we will compare the properties of satellite galaxies with those of central galaxies to

assess whether this affects their internal properties (see also Auger 2008). The connection with the mass profile at larger radii, as determined from a joint weak and strong lensing analysis (paper IV), will be examined in future work.

Figure 1 shows local overdensities versus global overdensities for the sample of lenses. Some of the lenses live in considerable overdensities, as may be expected for massive early-type galaxies.

As a final check, we used the NASA Extragalactic Database to look for known clusters in the vicinity of the lenses. We restricted our search to known clusters within 10 arcminutes, which is 20 times the typical Einstein radius of a massive cluster at these redshifts. We expect that the shear and convergence contributed by massive clusters more distant on the sky than 10 arcminutes will be less than 2.5 percent at the location of the lens, and even less for groups, assuming conservatively an isothermal profile. For comparison, this 10 arcminutes scale corresponds to approximately 2 Mpc at the typical redshift of the SLACS lenses ( $z \approx 0.2$ ), i.e. comparable to the virial radius of a large cluster where the shear is only a few percent (e.g., Kneib et al. 2003). Therefore, we can safely neglect the more distant clusters in the present analysis.

Table 1 lists for each match the name of the cluster, the distance on the sky in arc-minutes and the redshift of the cluster (if known). In case of multiple matches for one lens (frequently because the same cluster is identified by more than one survey), we list the clusters in increasing order of three-dimensional distance from the lens. clusters with no known redshift are listed last. We consider a cluster physically associated to a lens if the redshifts match to better than 0.02, where the interval is chosen to take into account the typical errors in photo- $z$  of SDSS based cluster searches (Koester et al. 2007). In support of the reliability of our environment measures, 12 of the 13 lenses associated with known clusters do lie in overdense regions. The highest overdensity is associated with lens J1143-0144 and the known cluster Abell 1364 (also identified by the C4 and MaxBCG surveys). The only exception is the lens J0252+0039, which is 6.6' from candidate group/cluster NSCSJ025225+003540 (estimated redshift  $z = 0.27$ ). The candidate cluster is only detected by one of the methods applied by Lopes et al. (2004) (Voronoi tessellation) and is not visible in the SDSS image of the field. We therefore consider this group/cluster identification as spurious and ignore it in the rest of the paper. Visual inspection of the SDSS images of the other 12 matches confirms their identification as groups/clusters.

### 3. ARE THE ENVIRONMENTS OF LENSES SPECIAL?

To quantify whether the environment of lenses are special, we compare in Figure 3 the distribution of normalized global and local galaxy density for the lenses and for the twins. To facilitate the comparison, the histogram for the twins has been renormalized to the number of lenses. Lens galaxies tend to live in overdense environments, both in terms of local and global measures, although the range is broad. This is expected due to the clustering of massive early-type galaxies (e.g., Davis & Geller 1976; Hogg et al. 2003; Coil et al. 2008; Meneux et al. 2008). However, the same holds for the twins. The distribu-

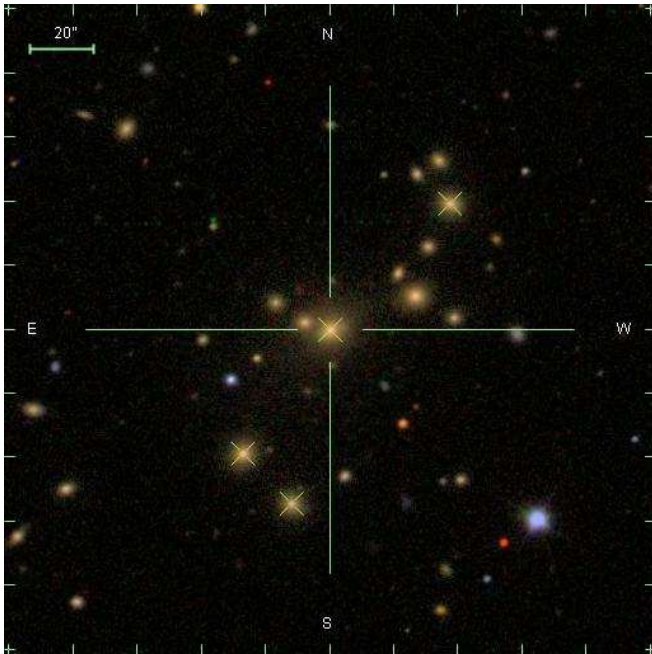


FIG. 2.— Field around the lens J1143-0144 as imaged by the SDSS. Spectroscopic targets are identified by crosses. North is up, East is left. The redshifts are consistent with that of the main lens (0.106; at the center of the field); from left to right they are 0.104, 0.106, 0.109).

tion of density measures appears to be indistinguishable for the two samples. The Kolmogorov-Smirnov statistic may suggest a marginal level of difference (the probability that  $\Sigma_{10}$  and  $D_1$  of the lenses and twins are drawn from the same distribution is  $\sim 8 - 9\%$ ). However, the average values do not seem to corroborate any difference: the mean local overdensity is somewhat larger for lenses than for twins (less than 68%CL), while the opposite is true for the global overdensity (at less than 95%CL). The distributions are skewed, with the average larger than the median due to the extended tail towards high densities. Therefore it is useful to compare the median and semi-quartile intervals, which are less sensitive to the tails of the distribution. The median (semi-interquartile intervals) of  $\Sigma_{10}/\langle\Sigma_{10}\rangle$  is 1.15 (0.59) for the lenses and 1.40 (0.94) for the twins. The median (semi-interquartile intervals) of  $D_1/\langle D_1\rangle$  is 0.90 (0.34) for the lenses and 1.03 (0.42) for the twins.

Thus, we conclude that – within the current measurement errors of our survey – lens galaxies live in the same environment as similar non-lens galaxies. Note that in principle our lenses are selected also on the basis of magnitude and colors, at least for the luminous red galaxies subset. However, our finding extends the conclusion of Papers II and V that the dominant parameter is velocity dispersion. Once velocity dispersion is matched, lenses are indistinguishable from “twins.” This is consistent with the tight correlation between velocity dispersion and global parameters of early-type galaxies (e.g., Bender et al. 1992). In conclusion, this result corroborates our previous findings that SLACS lens galaxies are an unbiased sample of massive early-type galaxies, and our working assumption that our lens-based results can be generalized to the overall population.

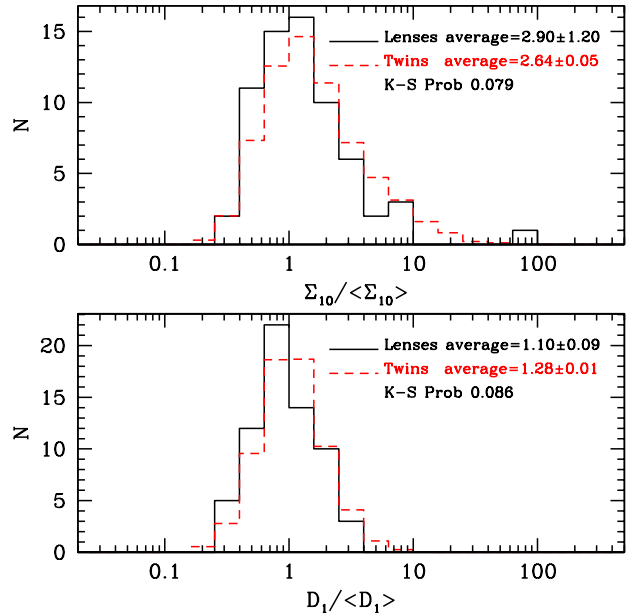


FIG. 3.— Distribution of overdensity of galaxies for the SLACS sample (solid histogram) and the control “twins” (dashed histogram). Two measures of environment are used: 1)  $\Sigma_{10}$  the number density within the area enclosing the ten nearest neighbors (upper panel); 2)  $D_1$  the number density of galaxies inside a cone of radius one  $h^{-1}$  Mpc. Both quantities are normalized to the average values for the universe using random lines of sight. Both lenses and twins are found in overdense regions as expected for massive early-type galaxies. However, the two distributions are statistically indistinguishable, as discussed in Section 3. Within the uncertainties, lenses live in the same environments as non-lens early-type galaxies.

#### 4. ENVIRONMENT AND INTERNAL STRUCTURE OF EARLY-TYPE GALAXIES

In this section, we investigate the dependence of the internal structure of lens galaxies on the environment. We first look in § 4.1 at the mis-alignment between mass and light, which we expect to increase with increasing local and global density as a result of the external potential associated with the large scale structure. In Section 4.2 we analyze the dependence of the slope of the mass density profile of the lens galaxy on environment, to probe tidal stripping of dark-matter halos. In Section 4.3 we study the run of projected mass with radius and the mass plane scaling law, in relation to the environment, as a probe of variations of internal structure and of extra mass associated with overdensities.

##### 4.1. Alignment of mass and light

In this section we compare the position angle of the best fit singular isothermal ellipsoid model with no external shear to the position angle of the light distribution. Because of the significance of the stellar contribution at the scales probed by the Einstein radii of SLACS lenses, we expect that the two will be aligned if there is no significant external potential. Vice-versa, the r.m.s. amplitude of the misalignment is a measure of the external perturbing potential (Keeton et al. 1997; Koopmans et al. 2006). In Paper III we used the small r.m.s. amplitude of the misalignment to show that the average external shear must be smaller than 0.035 (see also Paper VII).



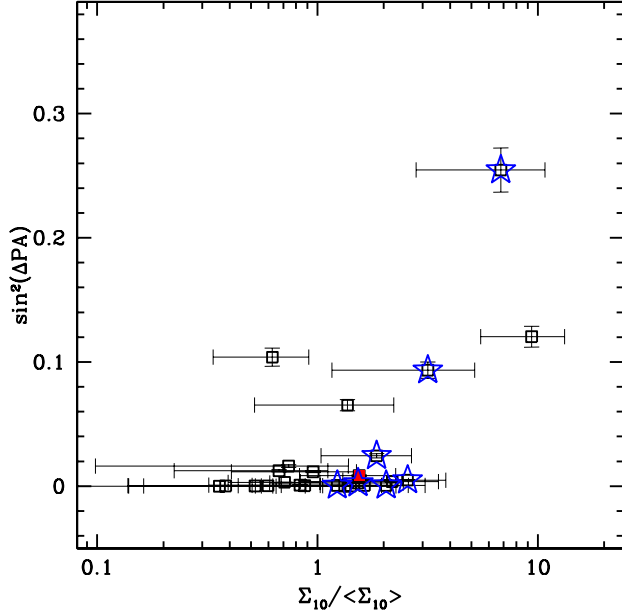


FIG. 4.— Misalignment between the major axis of the optical light and that of the best fitting singular isothermal ellipsoid ( $\Delta PA$ ) as a function of local overdensity. The subset of objects for which position angles can be accurately measured is shown (i.e. axis ratio of the optical light  $< 0.9$  and belonging to the “ring subsample” as described in Paper VII). As in the rest of the paper red solid symbols identify “satellite” lens galaxies while black empty symbols identify “central” lens galaxies. Blue empty stars identify lenses associated with known clusters. The misalignment observed in overdense regions can be explained as due to randomly aligned external shear of order  $\sim 0.06$ .

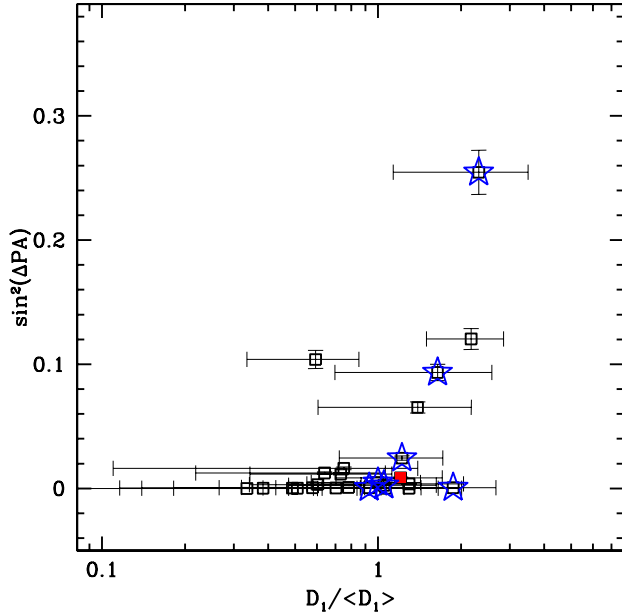


FIG. 5.— As in Figure 4 for global overdensity instead of local overdensity.

In this Section we investigate trends with the environment.

Figures 4 and 5 show the offset between the position angle of the light and that of the mass distribution as a function of the local and global overdensity. As discussed in Paper VII, the position angle can only be well measured if the light and mass distributions are not circular and the lens model provides sufficient constraints. Therefore, only the 25 objects with significant ellipticity (axis ratio  $< 0.9$ ) and with well measured mass PA (the “ring subset”) are shown.

The correlation between alignment and local and global environment is significant. Fitting for example a power law relation, we find  $\sin^2(\Delta PA) = (0.14 \pm 0.05) \log(D_1/\langle D_1 \rangle) + 0.03 \pm 0.01$  and  $\sin^2(\Delta PA) = (0.10 \pm 0.03) \log(\Sigma_{10}/\langle \Sigma_{10} \rangle) + 0.02 \pm 0.01$ .

We do not expect a simple relation between the two quantities, as a galaxy sitting right at the center of a cluster could in principle experience no external shear. However, in general, lenses in overdense environments will be more likely to be affected by nearby companions, causing a misalignment between the position angle of the stellar mass and that of the total gravitational potential, since the external perturber is presumably located in a random direction. Using Equation 22 from Keeton et al. (1997) we estimate that for the mean mass axis ratio of our sample  $(b/a)_{SIE} \approx 0.77$ , external shear of order 0.05-0.06 is needed to match the average observed  $\sin^2 \Delta PA \sim 0.1$  in the overdense regions, while external shear appears to be negligible in the underdense regions. Assuming that the external perturbers can be approximated to first order as singular isothermal spheres, this would mean that – even for the larger overdensities – the external contribution to the local surface mass density (convergence) is of order  $\lesssim 10\%$  within the Einstein radius of the main lens.

#### 4.2. Mass density profile

Figures 6 and 7 show  $f_{SIE}$  – the ratio between the central stellar velocity dispersion  $\sigma_*$  and that of the best fitting singular isothermal ellipsoid  $\sigma_{SIE}$  – as a function of the local and global overdensity. This ratio is a direct empirical measure of the local density slope, expected to be close to unity for isothermal profiles, larger than unity for steeper slopes and smaller than unity for flatter slopes (e.g., Treu & Koopmans 2002a, 2004). We thus use this quantity to study the effect of the environment on the local mass density slope of galaxies at kpc scales, since this is an excellent proxy for the total mass density slope  $\gamma'$  (such that  $\rho_{tot} \propto r^{-\gamma'}$ ) obtained from a full lensing and dynamical model (Koopmans et al. 2006). The full results of lensing and dynamical models will be presented in a forthcoming paper (Koopmans et al. 2008, in prep; hereafter Paper IX). Figure 8 shows the goodness of the proxy for the 58 objects in common between this study and Paper IX:  $\gamma' - 2 = (1.99 \pm 0.07)(f_{SIE} - 1) + (0.006 \pm 0.008)$  (see Figure 8), for isotropic models. It is important to emphasize that  $\sigma_*$  and  $\sigma_{SIE}$  are the input to determining  $\gamma'$  via a well defined set of equations (Koopmans 2005). Therefore, the errors are highly correlated along the direction of the best fit relation  $\delta\gamma'/\gamma' \sim \delta f_{SIE}/f_{SIE}$  and the range covered by both quantities in Figure 8 is a representation of the intrinsic scatter as well as the observational error. The small residual scatter in the transformation between  $\gamma'$  and  $f_{SIE}$  is due to the range of Einstein radius

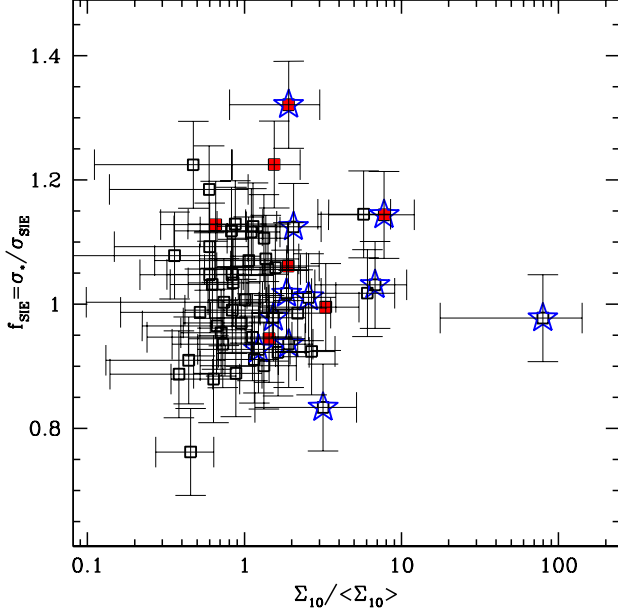


FIG. 6.— Ratio between central stellar velocity dispersion and that of the best fitting singular isothermal ellipsoid as a function of the local overdensity parameter. No significant correlation is found. “Satellite” lenses are indicated by red solid symbols, while black empty symbols indicate “central” galaxies.

to effective radius ratios spanned by the SLACS sample. Note also that this best fit transformation is obtained for isotropic models with Hernquist stellar profiles, and we expect it to be different for other types of models. Also, we would expect to find a different transformation when the average ratio between effective radius and Einstein radius is significantly different, e.g. for the LSD sample (Treu & Koopmans 2004). A comprehensive analysis of  $\gamma'$ , its statistical distribution and dependence on orbital parameters, as well as host galaxy properties, will be given in Paper IX.

The plots show two basic facts. First, the correlation between local and global and environment and  $f_{\text{SIE}}$  is not significant. Fitting a linear relation between  $f_{\text{SIE}}$  and the logarithm of the local and global overdensities gives slopes of  $0.02 \pm 0.03$  and  $0.10 \pm 0.06$  respectively. If it were present, a correlation would indicate that mass density profiles tend to be steeper in overdense environment perhaps as a result of tidal truncation of the galactic dark-matter halos by external fields (as suggested by some numerical simulations, e.g., Dobke et al. 2007). The lack of correlations suggests that either the effect is not strong enough to be detected at the kpc scales probed by the SLACS Einstein Radii given the uncertainties in both the local slope and the environment measures, or that the contribution of the environment to the projected mass density is sufficient to counterbalance the effect. This latter explanation, however, does not appear to be supported by the data, as the local density slope of the lenses belonging to known clusters is indistinguishable from that of the “isolated” central lenses (Figure 9).

Second, our result hints that the mass density profiles of “satellite” galaxies (identified by solid red points in the plots) may be steeper than those of “central” galaxies,

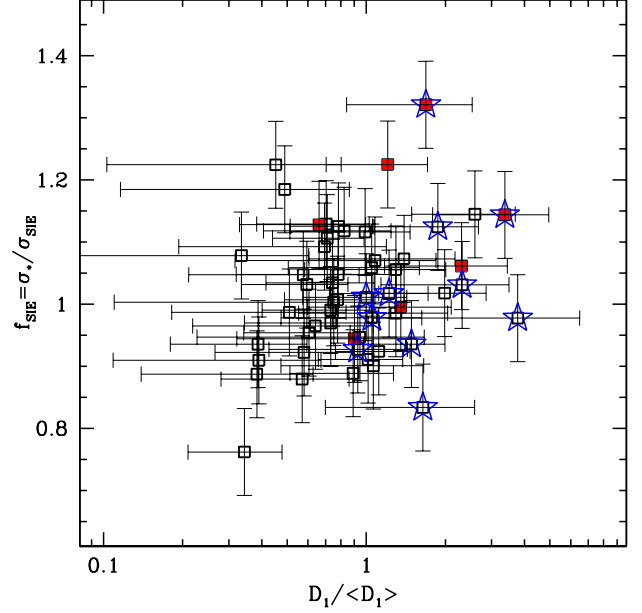


FIG. 7.— As in Figure 6 for global overdensity instead of local overdensity.

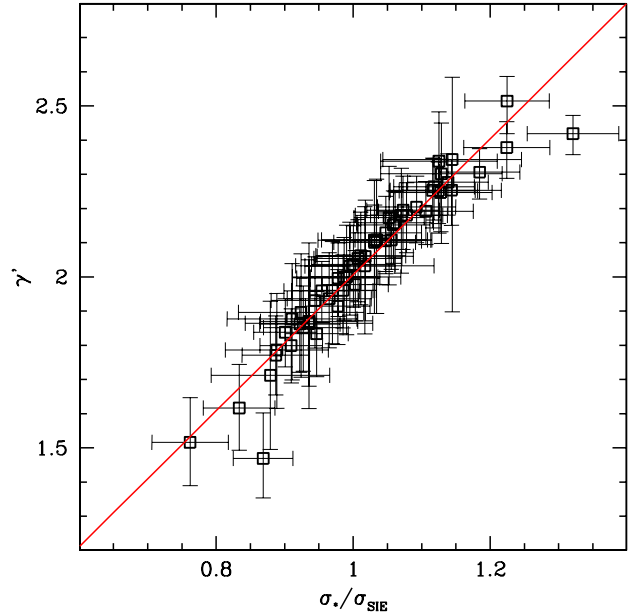


FIG. 8.— Transformation from  $f_{\text{SIE}}$  to slope of the total mass density profile  $\gamma'$  (from Paper IX, Koopmans et al. 2008). The best fit linear relation is shown as a solid red line:  $\gamma' - 2 = (1.99 \pm 0.07)(f_{\text{SIE}} - 1) + (0.006 \pm 0.008)$ .

consistent with the picture of tidal truncation (Figure 9). The average  $f_{\text{SIE}}$  is larger for “satellite” galaxies than for “central” galaxies (approximately at 95%CL). However, a K-S test shows that the probability that the two distributions are drawn from the same parent distribution is non-negligible (7.5%) and therefore we caution that this difference may not be significant. In this sense, and in

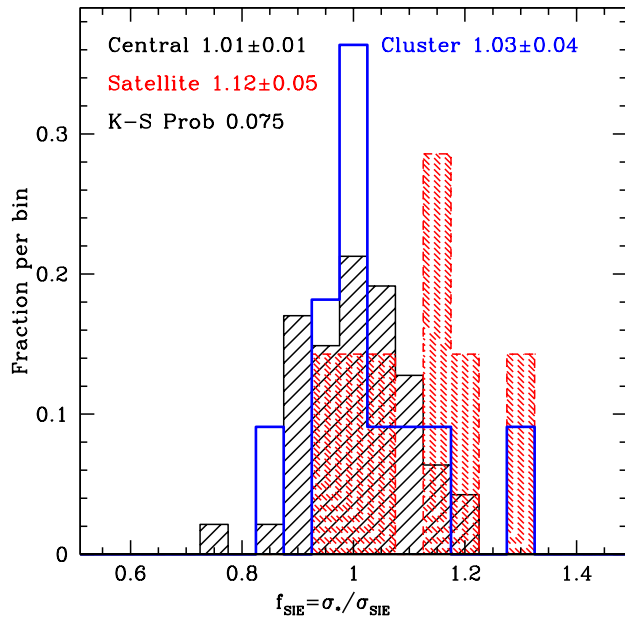


FIG. 9.— Distribution of the ratio between central stellar velocity dispersion and that of the best fitting singular isothermal ellipsoid for central (solid black histogram) and satellite (dashed red histogram) lens galaxies. Satellite lenses have somewhat steeper average density slopes. See § 4.2 for discussion.

terms of overall significance, our finding agrees with that reported by Auger (2008) who studied the initial SLACS sample of 15 lenses, finding tentative evidence for steeper mass density profiles in overdense regions. As we discuss in the next section, an alternative or possibly complementary explanation is that  $f_{\text{SIE}}$  is somewhat higher for the central galaxies as a result of an additional contribution to the lensing mass by the dark-matter halo of the overdensity.

#### 4.3. Enclosed mass, external convergence and the average mass-density structure of early-type galaxies

Finally, we study the radial dependence of mass enclosed within the Einstein radius as a function of local and global environment. As discussed in Paper VII, for an isolated galaxy described by a singular isothermal sphere total mass density profile, we expect the following relation:

$$\log \frac{M(< R)}{M_{\text{dim}}} = \log \frac{R}{R_e} + \log 2c_{e2}, \quad (1)$$

where  $M_{\text{dim}} = \sigma_{e,2}^2 R_e / 2G$  is the “dimensional” mass,  $\sigma_{e,2}$  is the stellar velocity dispersion corrected to an aperture of radius equal to half the effective radius  $R_e$ ,  $G$  is the gravitational constant, and  $c_{e2} \equiv \frac{2GM_{e2}}{R_e \sigma_{e,2}^2}$  – where  $M_{e2}$  is the projected mass enclosed by a circle of radius equal to one half the effective radius – is a dimensionless structure parameter that depends on the profile and anisotropy of the luminous tracer (Nipoti et al. 2008). As shown in Figure 10, Equation 1 is found to be a good description of the SLACS sample, with an intercept  $\log 2c_{e2} = 0.83 \pm 0.01$ . For typical luminosity profiles,

such as de Vaucouleurs (1948) with close to isotropic pressure tensor,  $\log c_{e2} \approx 0.57$  (Nipoti et al. 2008), consistent with the best fit value of the intercept of Equation 1. The dimensionless structure parameter can vary by as much as  $\sim 0.05$  dex within the realm of physically plausible galaxy models, reproducing the intrinsic scatter derived by Bolton et al. (2008b) on the basis of the mass plane analysis.

This description of the SLACS sample is approximately equivalent of that in the terms of the mass plane (MP) presented by Bolton et al. (2007, 2008b) and Nipoti et al. (2008), since Eq 1 evaluated at  $R = R_e/2$  returns an equation very close to that describing the mass plane.

We can use the scaling relation in Eq 1 to measure the effects of the environment in the form of an additional surface mass density<sup>10</sup>, i.e. external convergence in the language of gravitational lensing. If the lens galaxy can be described as an isothermal sphere plus a uniform surface mass density representing the first order expansion of the mass distribution along the line of sight from material not associated with the lens, the surface mass density profile of the lens becomes:

$$\kappa = \frac{1}{2} \frac{R_{\text{Ein},0}}{R} + \kappa_{\text{ext}}, \quad (2)$$

where the surface mass density  $\kappa$  is expressed as usual (e.g., Schneider 2006) in units of the critical density  $\Sigma_{\text{crit}} = \frac{c^2 D_s}{4\pi G D_d D_{ds}}$  ( $c$  is the speed of light,  $D_s$ ,  $D_d$ ,  $D_{ds}$  are the angular diameter distances from the observer to the source, from the observer to the lens, and between the lens and the source, respectively).  $R_{\text{Ein},0}$  is the Einstein radius that the galaxy would have if there was no external surface mass density contribution  $\kappa_{\text{ext}}$ .

If we were to neglect the presence of the external surface mass density and model the galaxy as an isolated isothermal sphere, we would infer the following Einstein radius and Einstein mass:

$$R_{\text{Ein}} = \frac{R_{\text{Ein},0}}{1 - \kappa_{\text{ext}}}; M_{\text{Ein}} = \frac{M_{\text{Ein},0}}{(1 - \kappa_{\text{ext}})^2}, \quad (3)$$

expressed in units of the corresponding quantities for the isolated lens. Using lensing alone we would not be able to detect the presence of the external surface mass density, due to the mass-sheet degeneracy (Falco et al. 1985; Kochanek 2006). However, the external surface mass density modifies Equation 1:

$$\log \frac{M_{\text{Ein}}}{M_{\text{dim}}} = \log \frac{R_{\text{Ein}}}{R_e} + \log 2c_{e2} - \log(1 - \kappa_{\text{ext}}), \quad (4)$$

obtained by combining Equations 3 and 1. Therefore we can in principle measure the external mass distribution using this scaling law<sup>11</sup>. Vertical offsets from the average relation in Figure 10

<sup>10</sup> To avoid duplication, we only describe the trends of Equation 1 with environment, the trends of the MP being effectively indistinguishable and less straightforward to interpret.

<sup>11</sup> This procedure is similar to that adopted by Koopmans et al. (2003) and Suyu et al. (2008) to break the mass-sheet degeneracy in measuring the Hubble constant by relying on stellar velocity dispersion measurements.



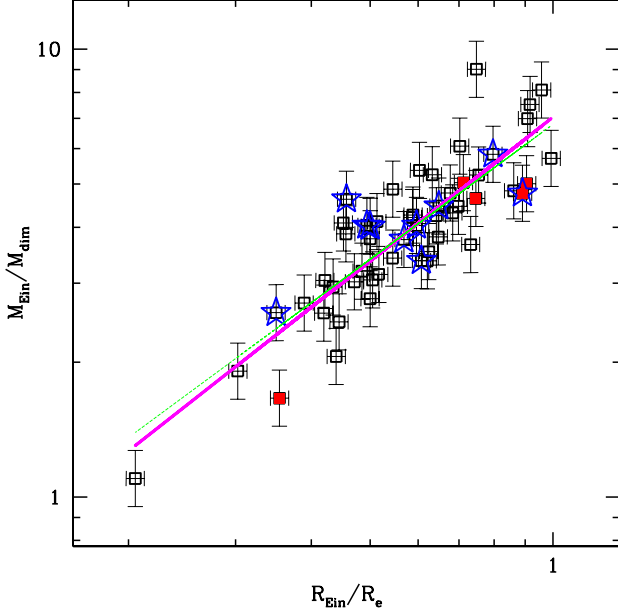


FIG. 10.— Projected mass inside the Einstein radius, normalized by dimensional mass, as a function of the Einstein radius in units of the effective radius. For an isothermal model a linear relation is expected (thin dotted green line; Bolton et al. 2008b). The best fit line (thick solid magenta line) is consistent with a linear relation. Symbols, as in the other figures, identify satellite galaxies (red filled squares) and galaxies associated with known clusters (blue open stars).

$$\Delta \log \frac{M_{\text{Ein}}}{M_{\text{dim}}} = \log \frac{M_{\text{Ein}}}{M_{\text{dim}}} - \log \frac{R_{\text{Ein}}}{R_e} - 0.83, \quad (5)$$

can be interpreted as due to the environment if  $c_{e2}$  is constant. Note however that there is a degeneracy between the dimensionless structure parameter  $c_{e2}$  and  $\kappa_{\text{ext}}$ , which should be kept in mind while interpreting any trend.

To quantify any trends we show the offset from the average relation as a function of local and global overdensity in Figure 11. No significant correlation is found, suggesting that any environmental effect is smaller than our measurement errors. The slope of the relations  $\Delta \log M_{\text{Ein}}/M_{\text{dim}} = \eta_{1,\Sigma_{10}} \log \Sigma_{10}/\langle \Sigma_{10} \rangle + \eta_{0,\Sigma_{10}}$  and  $\Delta \log M_{\text{Ein}}/M_{\text{dim}} = \eta_{1,D_1} \log D_1/\langle D_1 \rangle + \eta_{0,D_1}$  are consistent with zero:  $\eta_{1,\Sigma_{10}} = -0.01 \pm 0.03$  and  $\eta_{1,D_1} = -0.07 \pm 0.05$ . Thus, even in the highest density environments ( $\Sigma_{10}/\langle \Sigma_{10} \rangle \sim 100$ ;  $D_1/\langle D_1 \rangle \sim 10$ ), we do not expect the external contribution to the total mass to be more than 0.03 dex and 0.06 dex respectively, at the 95% CL, corresponding to external mass surface densities of less than  $\kappa_{\text{ext}} \sim 0.07$  and  $\kappa_{\text{ext}} \sim 0.13$ , assuming that the dimensionless structure parameter is independent of environment.

Considering special subclasses of objects, the satellite galaxies are below the average ( $\langle \Delta M_{\text{Ein}}/M_{\text{dim}} \rangle_{\text{sat}} = -0.07 \pm 0.03$  dex; the difference with respect to central galaxies being  $-0.09 \pm 0.03$ ), while the galaxies in known clusters are consistent with the average ( $\langle \Delta M_{\text{Ein}}/M_{\text{dim}} \rangle_{\text{clu}} = 0.02 \pm 0.02$ ). These offsets could be interpreted as a combination of two effects: i) negative

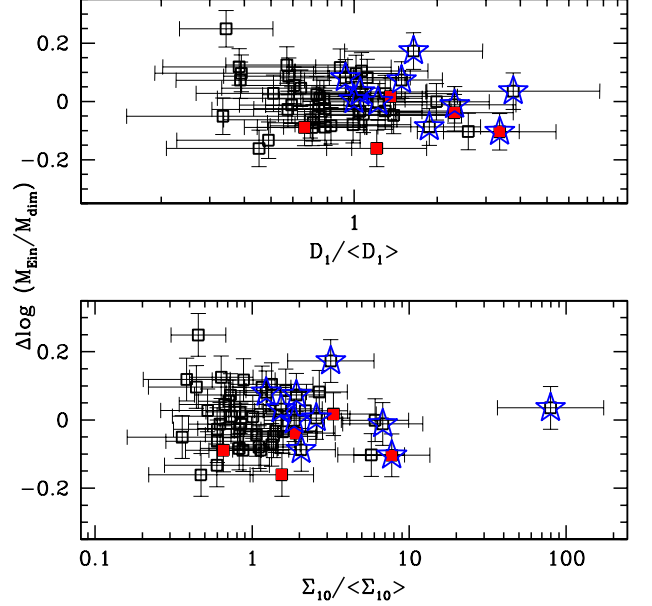


FIG. 11.— Residuals from the isothermal scaling ( $\Delta \log M_{\text{Ein}}/M_{\text{dim}}$ ) as a function of local (bottom) and global (top) overdensity. Symbols, as in the other figures, identify satellite galaxies (red filled squares) and galaxies associated with known clusters (blue open stars).

external mass contributions for the satellites (negative  $\kappa_{\text{ext}}$ ), i.e. satellite galaxies living in underdense regions; ii) different  $c_{e2}$  for satellite and central galaxies. Consistent with the analysis of the results presented in § 4.2, it seems that the most plausible interpretation of the offset between the satellite and central galaxies is the latter. This could arise for example from systematic changes of their internal structure due to tidal stripping of their dark-matter halos. However, a combination of the two effects cannot be ruled out without more information, e.g. from spatially resolved stellar kinematics (Czoske et al. 2008).

The intrinsic scatter around the best fit relation (0.059 dex along the vertical axis) is also of interest, because it allows us to set limits to the combined degree of inhomogeneity in the internal structure of the lens galaxies and on the external mass surface density. Nipoti et al. (2008) used the small internal scatter of the relation to constrain  $\log c_{e2}$  and thus the internal structure of the lenses, neglecting the effects of external mass along the line of sight. Considering that part of the scatter may be due to fluctuations in external mass along the line of sight it is likely that this is an upper limit to degree of inhomogeneity of the internal structure of early-type galaxies. Conversely, if we were to postulate that lens galaxies are absolutely homogeneous in their internal structure, the observed internal structure would imply an r.m.s. scatter of 0.05 dex in  $\log(1 - \kappa_{\text{ext}})$ , i.e.  $\sim 0.1$  in  $\kappa_{\text{ext}}$ . We can therefore take this number as an upper limit to the r.m.s contribution of the external potential, in line with the expectations of theoretical calculations for image separations of order one arcsecond (Oguri et al. 2005).

## 5. DISCUSSION

Our study addresses two issues which have gathered significant attention in the literature in the past few years: i) the role of the environment in the modeling and interpretation of gravitational lensing results; ii) the role of environment in shaping the structure and dynamics of galaxies.

As far as the first issue is concerned, we find that lens galaxies tend to live preferentially in overdense regions. As pointed out by a number of authors, this is expected since gravitational lenses are typically massive galaxies and are therefore clustered. In fact, one of the main results of this paper is that the distribution of environments for lens galaxies and “twins” selected to have the same velocity dispersions and redshifts are indistinguishable within the errors. This conclusion extends our previous finding that *SLACS lenses are normal galaxies* that just happen to be well aligned with a background source.

Defining membership in groups/clusters either by the association of lens galaxies with group/clusters known to NED or by (somewhat arbitrary) cuts in overdensity ( $D_1/\langle D_1 \rangle > 1$  and  $\Sigma_{10}/\langle \Sigma_{10} \rangle > 2$ ) we find that approximately 20% of the SLACS lenses belong to a group/cluster ( $12/70 = 17 \pm 5\%$  and  $13/66 = 20 \pm 6\%$ , respectively, according to the two definitions). This is in line with the theoretical estimates by Keeton et al. (2000) and somewhat lower than suggested by spectroscopic and photometric studies of other samples of lenses, typically at higher redshift (Fassnacht & Lubin 2002; Momcheva et al. 2006; Auger et al. 2007; Fassnacht et al. 2007; Williams et al. 2008), although a direct comparison of the fraction is difficult because of the different definitions of groups/clusters adopted by various studies.

In addition, we find that the contribution of the environment to the potential of the SLACS lenses is small, typically undetected, reaching 10-20 % in surface mass density (corresponding to external shear and convergence of order 0.05-0.10) only for a few extreme cases. This is consistent with our previous studies that showed that SLACS lenses can be successfully modeled by singular isothermal spheres without external shear, and at variance with other sample of lenses where substantial amounts of external shear are required for successful models (e.g. Hogg & Blandford 1994; Keeton et al. 1997; Moustakas et al. 2007). Our result is also in disagreement with the study by Guimarães & Sodr  (2007) who suggested significant external convergence for the SLACS sample based on simple one-component models (i.e. light traces mass), which are also ruled out by a number of other arguments as discussed in previous SLACS papers.

The reduced role of the environment in the SLACS lenses with respect to other samples of lenses is likely to be due to the lower redshift of lens and source and consequently to the smaller Einstein radii both in terms of angular scales ( $\langle R_{\text{Ein}} \rangle = 1''.2$ ) and in terms of physical scales of the lens galaxies, typically half the effective radius as opposed, e.g., to a few effective radii for the lenses studied by the LSD project (Treu & Koopmans 2004) and the typical CASTLES lenses (Rusin et al. 2003). In addition, the SDSS fiber selection imposes effectively an upper cutoff to the image separation, corresponding to  $\lesssim 2''$  (see discussion in Dobler et al. 2008), in order for a sizeable fraction of the lensed flux to be captured by the spectrograph. The two effects work in the same di-

rection, increasing the relative importance of the stellar mass for the lens model with respect with other sample of lenses and ruling out the largest image separation lenses where the effects of group and cluster environments are expected to be largest (Oguri et al. 2005). The low level of environmental contribution to the lens potential is a major benefit of the SLACS sample, reducing the risk of biased inferences on the structure of the lenses due to poor modeling of the environment (Keeton & Zabludoff 2004). For example, if time variable phenomena are identified in the SLACS lensed sources (e.g. active nuclei or supernovae) they would make excellent systems to determine the Hubble constant from gravitational time delays.

The environment and the distortion caused by external shear has often been considered one of the potential solutions to the so-called “quad problem” (Rusin & Tegmark 2001; Holder & Schechter 2003), i.e. the abundance of the quadruply imaged lenses amongst radio-selected lenses (9/22 in the CLASS survey, plus one system with six images; Browne et al. (2003)). The “quad-problem” is not observed for optically selected multiply imaged quasars (Oguri 2007), suggesting that the faint end slope of the luminosity function of the sources is different for radio and optically selected sources. The classification in doubles and quads is not so clear cut for SLACS, because of the extended nature and sometimes multiple components of the sources. However, if we base our classification on the criterion that the peak of the brightest source being inside or “on” the inner caustic, only 9/70 ( $13 \pm 5\%$ ) SLACS lenses are classified as quads<sup>12</sup>, significantly lower than the radio selected samples. Qualitatively, this is in line with the expectations of models that do not require large amounts of external shear (e.g., Rusin & Tegmark 2001; Oguri 2007). However, a full modeling of the SLACS source distribution and selection function is required for a quantitative comparison. This is left for future work, when we will analyze the properties of the source galaxies in more detail.

As far as the second issue is concerned, we do not find significant correlations between the internal properties of the lens galaxies and the environment. The only difference, detected at 2-3  $\sigma$  significance, is between central and satellite galaxies, in the sense that the latter have somewhat steeper mass density profiles than the former do. We argue that this may be interpreted as due to tidal truncation of the outer parts of the galaxies, as suggested by numerical (Dobke et al. 2007) and observational studies (Impey et al. 1998; Treu & Koopmans 2002b; Auger 2008). This finding extends at smaller scales previous evidence for tidal truncation at larger radii, based on the weak galaxy-galaxy lensing signal (Natarajan et al. 2002b; Gavazzi et al. 2004; Natarajan et al. 2007). However, current data cannot exclude the possibility that this trend is in part due to an extra amount of convergence from the larger-scale structure around central galaxies. In the future, we hope to break this degeneracy with high quality spatially resolved kinematics. In any case,

<sup>12</sup> The lenses were classified independently by T.T. and A.S.B.. The nine “consensus” quads are: J0405-0455, J0737+3216, J0912+0029, J0946+1006, J0956+5100, J1100+5329, J1106+5228, J1402+6321, J1420+6019, J2300+0022. Three additional lenses are classified as quads by only one of two classifiers, J0956+5100, J1103+5322, J2341+0000, possibly increasing the fraction to 12/70, i.e.  $17 \pm 5\%$

the small intrinsic scatter in the slope of the mass density profiles and around Equation 1 (or equivalently the MP) shows that SLACS lenses are both highly homogeneous in their internal structure and suffer from little contamination by large scale structures along the line of sight.

A limitation of this study is the reliance on photometric catalog of galaxies as tracers of the environment. X-ray data and spectroscopic redshifts for a substantial fraction of the objects in each field are needed to make further progress, by providing accurate position and masses for the groups and clusters in the vicinity of the lens and therefore an independent estimate of the external convergence and shear. X-ray data in particular would be needed to detect fossil groups.

## 6. SUMMARY AND CONCLUSIONS

We have used the SDSS database to measure the environment around seventy strong gravitational lens galaxies selected from the SLACS Survey. We adopt two standard estimators: the surface density of galaxies within the tenth nearest neighbor ( $\Sigma_{10}$ ) and the density of galaxies within a cone of radius one  $h^{-1}$  Mpc ( $D_1$ ). Both are normalized in terms of the corresponding quantities for random fields, and are referred to as “local” and “global” overdensities. For comparison purposes, we also selected from the SDSS database a sample of 100 “twins” for each lens galaxy, i.e. galaxies with virtually the same redshift and velocity dispersion. The new observables are combined with measurements of internal properties of the lens galaxies from SLACS papers to investigate the relationship between early-type galaxy structure and environment. The main results of this study can be summarized as follows:

1. SLACS lens galaxies live generally in overdense environments. Twelve of the seventy lenses ( $17 \pm 5\%$ ) are associated with known clusters/groups at the same redshifts. This is consistent with the notion that lens galaxies are massive and therefore clustered.
2. The distribution of overdensities for SLACS lens galaxies is consistent within the errors with the corresponding distribution for “twin” non-lens galaxies. This is consistent with lens galaxies being an unbiased population of massive early-type galaxies with respect to their environment.
3. The misalignment of mass and light is found to correlate with the local overdensity of galaxies. The misalignment is negligible for most lens galaxies except for those in the most overdense regions. Randomly oriented external shear of order of 0.05-0.06 is required to reproduce the observed misalignment in the most overdense environments.
4. The small departures from the average relation between Einstein mass scaled by dimensional mass, and Einstein radius scaled by the effective radius support the previous conclusions. The contribution of the environment to the local potential of the main lens is estimated to be below the current detection threshold for most lenses except for those residing in the densest environments where it can

reach at most 10-20% in terms of surface mass density at the Einstein radius (0.05-0.1 external convergence).

5. No significant correlation is found between local and global overdensity and measures of internal structure, such as the slope of the total mass density profile—quantified in terms of  $f_{\text{SIE}}$ —and the difference between the observed Einstein mass and that predicted based on dimensional mass, effective radius, and Einstein radius. Thus – within the current level of precision – the internal structure of early-type galaxies does not appear to be biased by projection effects.
6. The properties of “satellite” galaxies (i.e., those with a nearby companion with  $i' < i'_{\text{lens}} - 1$ ) are found to be different than those of “central” galaxies at the 95-99% CL. The average slope of the total mass density profile is  $f_{\text{SIE}} = 1.12 \pm 0.05$  for the satellites and  $1.01 \pm 0.01$  for the central galaxies. Similarly, the ratio between Einstein Mass and  $M_{\text{dim}}$  — as a function of the Einstein radius in units of the effective radius ratio — is  $0.09 \pm 0.03$  dex lower for the satellites with respect to the central galaxies. This suggests that the outer parts of satellite galaxies are perturbed by the environment down to the kpc scales probed by strong lensing, consistent with tidal stripping.

We thank Steve Allen, Matt Auger, Maruša Bradač, and Chris Fassnacht for many insightful conversations. Support for programs #10174, #10587, #10886, #10494, #10798 was provided by NASA through a grant from the Space Telescope Science Institute, which is operated by the Association of Universities for Research in Astronomy, Inc., under NASA contract NAS 5-26555. T.T. acknowledges support from the NSF through CAREER award NSF-0642621, by the Sloan Foundation through a Sloan Research Fellowship, and by the Packard Foundation through a Packard Fellowship. L.V.E.K. is supported (in part) through an NWO-VIDI program subsidy (project number 639.042.505). The work of L.A.M. was carried out at the Jet Propulsion Laboratory, California Institute of Technology, under a contract with NASA. This research has made use of the NASA/IPAC Extragalactic Database (NED) which is operated by the Jet Propulsion Laboratory, California Institute of Technology, under contract with the National Aeronautics and Space Administration. This project would not have been feasible without the extensive and accurate database provided by the Digital Sloan Sky Survey (SDSS). Funding for the creation and distribution of the SDSS Archive has been provided by the Alfred P. Sloan Foundation, the Participating Institutions, the National Aeronautics and Space Administration, the National Science Foundation, the U.S. Department of Energy, the Japanese Monbukagakusho, and the Max Planck Society. The SDSS Web site is <http://www.sdss.org/>. The SDSS is managed by the Astrophysical Research Consortium (ARC) for the Participating Institutions. The Participating Institutions are The University of Chicago,

Fermilab, the Institute for Advanced Study, the Japan Participation Group, The Johns Hopkins University, the Korean Scientist Group, Los Alamos National Laboratory, the Max-Planck-Institute for Astronomy (MPIA), the Max-Planck-Institute for Astrophysics (MPA), New

Mexico State University, University of Pittsburgh, University of Portsmouth, Princeton University, the United States Naval Observatory, and the University of Washington.

## REFERENCES

- Abell, G. O., Corwin, Jr., H. G., & Olowin, R. P. 1989, *ApJS*, 70, 1
- Adelman-McCarthy, J., et al. 2008, *ApJS*, 175, 297
- Auger, M. W. 2008, *MNRAS*, 383, L40
- Auger, M. W., Fassnacht, C. D., Abrahamse, A. L., Lubin, L. M., & Squires, G. K. 2007, *AJ*, 134, 668
- Balogh, M., et al. 2004, *MNRAS*, 348, 1355
- Bender, R., Burstein, D., & Faber, S. M. 1992, *ApJ*, 399, 462
- Bolton, A. S., Burles, S., Koopmans, L. V. E., Treu, T., Gavazzi, R., Moustakas, L. A., Wayth, R., & Schlegel, D. 2008a, *ApJ*, in press, arXiv:astro-ph/0805.1931
- Bolton, A. S., Burles, S., Koopmans, L. V. E., Treu, T., & Moustakas, L. A. 2006, *ApJ*, 638, 703
- Bolton, A. S., Burles, S., Treu, T., Koopmans, L. V. E., & Moustakas, L. A. 2007, *ApJ*, 665, L105
- Bolton, A. S., Treu, T., Koopmans, L. V. E., Gavazzi, R., Moustakas, L. A., Burles, S., Schlegel, D., & Wayth, R. 2008b, *ApJ*, in press, arXiv:astro-ph/0805.1932
- Browne, I. W. A., et al. 2003, *MNRAS*, 341, 13
- Capak, P., Abraham, R. G., Ellis, R. S., Mobasher, B., Scoville, N., Sheth, K., & Koekemoer, A. 2007, *ApJS*, 172, 284
- Coil, A. L., et al. 2008, *ApJ*, 672, 153
- Cooper, M. C., Newman, J. A., Madgwick, D. S., Gerke, B. F., Yan, R., & Davis, M. 2005, *ApJ*, 634, 833
- Cooper, M. C., et al. 2006, *MNRAS*, 370, 198
- . 2008, *MNRAS*, 383, 1058
- Csabai, I., et al. 2003, *AJ*, 125, 580
- Czoske, O., Barnabè, M., Koopmans, L. V. E., Treu, T., & Bolton, A. S. 2008, *MNRAS*, 384, 987
- Davis, M., & Geller, M. J. 1976, *ApJ*, 208, 13
- de Vaucouleurs, G. 1948, *Annales d'Astrophysique*, 11, 247
- Dobke, B. M., King, L. J., & Fellhauer, M. 2007, *MNRAS*, 377, 1503
- Dobler, G., Keeton, C. R., Bolton, A. S., & Burles, S. 2008, *ApJ*, submitted, astro-ph/803.2243
- Dressler, A. 1980a, *ApJS*, 42, 565
- . 1980b, *ApJ*, 236, 351
- Dressler, A., Oemler, A. J., Couch, W. J., Smail, I., Ellis, R. S., Barger, A., Butcher, H., Poggianti, B. M., & Sharples, R. M. 1997, *ApJ*, 490, 577
- Falco, E. E., Gorenstein, M. V., & Shapiro, I. I. 1985, *ApJ*, 289, L1
- Fassnacht, C. D., Kocevski, D. D., Auger, M. W., Lubin, L. M., Neureuther, J. L., Jeltama, T. E., Mulchaey, J. S., & McKean, J. P. 2007, *ApJ*, submitted, 711
- Fassnacht, C. D., & Lubin, L. M. 2002, *AJ*, 123, 627
- Gavazzi, R., Mellier, Y., Fort, B., Cuillandre, J.-C., & Dantel-Fort, M. 2004, *A&A*, 422, 407
- Gavazzi, R., Treu, T., Koopmans, L. V. E., Bolton, A. S., Moustakas, L. A., Burles, S., & Marshall, P. J. 2008, *ApJ*, 677, 1046
- Gavazzi, R., Treu, T., Rhodes, J. D., Koopmans, L. V. E., Bolton, A. S., Burles, S., Massey, R. J., & Moustakas, L. A. 2007, *ApJ*, 667, 176
- Goto, T., Sekiguchi, M., Nichol, R. C., Bahcall, N. A., Kim, R. S. J., Annis, J., Ivezić, Ž., Brinkmann, J., Hennesy, G. S., Szokoly, G. P., & Tucker, D. L. 2002, *AJ*, 123, 1807
- Goto, T., Yamauchi, C., Fujita, Y., Okamura, S., Sekiguchi, M., Smail, I., Bernardi, M., & Gomez, P. L. 2003, *MNRAS*, 346, 601
- Guimarães, A. C. C., & Sodr , L. J. 2007, astro-ph/07063098, 706
- Hogg, D. W., & Blandford, R. D. 1994, *MNRAS*, 268, 889
- Hogg, D. W., et al. 2003, *ApJ*, 585, L5
- . 2004, *ApJ*, 601, L29
- Holder, G. P., & Schechter, P. L. 2003, *ApJ*, 589, 688
- Impey, C. D., Falco, E. E., Kochanek, C. S., Leh r, J., McLeod, B. A., Rix, H.-W., Peng, C. Y., & Keeton, C. R. 1998, *ApJ*, 509, 551
- Keeton, C. R., Christlein, D., & Zabludoff, A. I. 2000, *ApJ*, 545, 129
- Keeton, C. R., Kochanek, C. S., & Seljak, U. 1997, *ApJ*, 482, 604
- Keeton, C. R., & Zabludoff, A. I. 2004, *ApJ*, 612, 660
- Kneib, J.-P., et al. 2003, *ApJ*, 598, 804
- Kochanek, C. S. 2002, *ApJ*, 578, 25
- . 2006, Part 2: Strong gravitational lensing, ed. G. Meylan, P. Jetzer, P. North, P. Schneider, C. S. Kochanek, & J. Wambsganss, 91–268
- Koester, B. P., et al. 2007, *ApJ*, 660, 239
- Koopmans, L. V. E. 2005, *MNRAS*, 363, 1136
- Koopmans, L. V. E., Treu, T., Bolton, A. S., Burles, S., & Moustakas, L. A. 2006, *ApJ*, 649, 599
- Koopmans, L. V. E., Treu, T., Fassnacht, C. D., Blandford, R. D., & Surpi, G. 2003, *ApJ*, 599, 70
- Lane, K. P., Gray, M. E., Arag n-Salamanca, A., Wolf, C., & Meisenheimer, K. 2007, *MNRAS*, 378, 716
- Lopes, P. A. A., de Carvalho, R. R., Gal, R. R., Djorgovski, S. G., Odewahn, S. C., Mahabal, A. A., & Brunner, R. J. 2004, *AJ*, 128, 1017
- Meneux, B., et al. 2008, *A&A*, 478, 299
- Miller, C. J., et al. 2005, *AJ*, 130, 968
- Momcheva, I., Williams, K., Keeton, C., & Zabludoff, A. 2006, *ApJ*, 641, 169
- Moran, S. M., Miller, N., Treu, T., Ellis, R. S., & Smith, G. P. 2007, *ApJ*, 659, 1138
- Moustakas, L. A., et al. 2007, *ApJ*, 660, L31
- Natarajan, P., Kneib, J.-P., & Smail, I. 2002a, *ApJ*, 580, L11
- Natarajan, P., Kneib, J.-P., Smail, I., Treu, T., Ellis, R., Moran, S., Limousin, M., & Czoske, O. 2007, *ApJ*, submitted, astro-ph/0711.4587, 711
- Natarajan, P., Loeb, A., Kneib, J.-P., & Smail, I. 2002b, *ApJ*, 580, L17
- Nipoti, C., Treu, T., & Bolton, A. 2008, *MNRAS*, submitted, astro-ph/0806.0570
- Oguri, M. 2007, *New Journal of Physics*, 9, 442
- Oguri, M., Keeton, C. R., & Dalal, N. 2005, *MNRAS*, 364, 1451
- Postman, M., & Geller, M. J. 1984, *ApJ*, 281, 95
- Postman, M., et al. 2005, *ApJ*, 623, 721
- Rusin, D., & Tegmark, M. 2001, *ApJ*, 553, 709
- Rusin, D., et al. 2003, *ApJ*, 587, 143
- Schneider, P. 2006, Part 1: Introduction to gravitational lensing and cosmology, ed. G. Meylan, P. Jetzer, P. North, P. Schneider, C. S. Kochanek, & J. Wambsganss, 1–89
- Smith, G. P., Treu, T., Ellis, R. S., Moran, S. M., & Dressler, A. 2005, *ApJ*, 620, 78
- Suyu, S. H., Marshall, P. J., Blandford, R. D., Fassnacht, C. D., Koopmans, L. V. E., McKean, J. P., & Treu, T. 2008, *ArXiv e-prints*, 804
- Treu, T., Ellis, R. S., Kneib, J.-P., Dressler, A., Smail, I., Czoske, O., Oemler, A., & Natarajan, P. 2003, *ApJ*, 591, 53
- Treu, T., Koopmans, L. V., Bolton, A. S., Burles, S., & Moustakas, L. A. 2006, *ApJ*, 640, 662
- Treu, T., & Koopmans, L. V. E. 2002a, *ApJ*, 575, 87
- . 2002b, *MNRAS*, 337, L6
- . 2004, *ApJ*, 611, 739
- Williams, K. A., Momcheva, I., Keeton, C. R., Zabludoff, A. I., & Leh r, J. 2008, *ApJ*, 672, 733
- Zwicky, F., Herzog, E., & Wild, P. 1961

TABLE 1  
SUMMARY OF RELEVANT MEASUREMENTS

Lens (1)	$z_l$ (2)	$\sigma_*$ (3)	$\sigma_{SIE}$ (4)	$\Sigma_{10}$ (5)	$\langle \Sigma_{10} \rangle_t$ (6)	$D_1$ (7)	$\langle D_1 \rangle$ (8)	$\langle D_1 \rangle_t$ (9)	Cluster Name (10)	$z_{cl}$ (11)	Dist (12)
J0008-0004	0.440	—	271	3.8±1.2	10.1±2.1	3.1±0.7	4.2±0.1	4.4±0.3	SDSSCEJ002.090289-00.168613	0.254	7.60
J0029-0055	0.227	245±19	217	3.3±1.0	6.5±0.7	2.7±0.6	3.8±0.1	3.8±0.2	None	—	—
J0037-0942	0.195	299±15	285	1.8±0.6	8.4±1.2	1.7±0.5	3.0±0.2	3.8±0.2	None	—	—
J0044+0113	0.120	283±14	269	—	—	—	—	—	ZwCl0041.9+0052	—	7.90
J0109+1500	0.294	274±21	243	4.5±1.4	6.4±0.7	3.1±0.7	4.0±0.1	3.5±0.1	None	—	—
J0157-0056	0.513	—	269	12.1±3.8	6.4±0.7	8.3±1.1	3.5±0.1	3.4±0.1	SDSSCEJ029.619265-00.943160	0.424	7.40
J0216-0813	0.332	354±24	347	9.5±3.0	7.6±1.0	3.1±0.7	1.6±0.1	4.0±0.2	None	—	—
J0252+0039	0.280	179±13	235	2.3±0.7	7.6±1.1	1.7±0.5	5.0±0.1	4.7±0.3	None	—	—
J0330-0020	0.351	232±23	252	11.6±3.7	6.4±0.5	4.8±0.9	4.3±0.1	4.1±0.2	None	—	—
J0405-0455	0.075	175±9	177	3.8±1.2	6.4±0.7	3.7±0.8	7.3±0.4	3.5±0.1	None	—	—
J0728+3835	0.206	231±12	256	5.1±1.6	7.9±0.9	4.1±0.8	3.8±0.2	4.3±0.2	None	—	—
J0737+3216	0.322	358±18	292	3.4±1.1	7.7±1.1	2.7±0.6	2.2±0.1	4.0±0.2	None	—	—
J0808+4706	0.220	—	—	1.2±0.4	8.1±1.0	1.1±0.4	2.3±0.1	3.8±0.2	None	—	—
J0822+2652	0.241	279±16	271	2.1±0.7	9.4±1.1	2.0±0.6	3.4±0.1	4.2±0.2	None	—	—
J0841+3824	0.116	235±11	248	3.2±1.0	10.2±1.5	2.7±0.6	2.8±0.2	4.7±0.3	MaxBCGJ130.27341+38.53306	0.240	9.00
J0903+4116	0.430	—	293	24.9±7.9	6.8±0.6	5.8±0.9	2.7±0.1	3.6±0.1	None	—	—
J0912+0029	0.164	341±17	346	5.5±1.7	12.1±1.8	3.3±0.7	2.5±0.1	4.3±0.2	None	—	—
J0935-0003	0.347	413±36	361	8.3±2.6	9.4±1.1	3.7±0.8	1.4±0.1	4.5±0.2	None	—	—
J0936+0913	0.190	260±13	243	4.8±1.5	9.3±1.3	4.8±0.9	3.5±0.2	4.4±0.3	MaxBCGJ143.87624+09.27139	0.127	8.00
J0946+1006	0.222	281±22	283	3.4±1.1	7.4±0.9	3.0±0.7	4.1±0.2	3.9±0.2	MaxBCGJ146.87912+10.07800	0.151	8.70
J0955+0101	0.111	211±14	224	7.7±2.4	10.5±2.7	4.8±0.9	5.4±0.3	4.6±0.5	SDSSCEJ148.948990+01.050020	0.311	7.10
J0956+5100	0.241	358±18	318	5.0±1.6	7.9±0.9	4.5±0.8	2.4±0.1	3.6±0.2	MaxBCGJ149.12403+51.00178	0.235	0.00
J0959+4416	0.237	262±20	254	2.8±0.9	7.4±0.9	2.5±0.6	3.4±0.1	3.9±0.2	None	—	—
J0959+0410	0.126	215±14	216	17.5±5.5	6.8±0.8	7.2±1.1	5.3±0.3	4.7±0.3	NSCJ095952+040356	0.153	6.70
J1016+3859	0.168	269±14	253	8.4±2.6	7.4±0.9	10.1±1.3	4.4±0.2	3.9±0.2	NSCJ101706+390221	0.206	8.60
									ABELL0963	0.206	9.30
									NSCSJ101645+385041	0.230	9.40
J1020+1122	0.282	306±20	304	3.2±1.0	7.1±0.8	2.5±0.6	3.2±0.1	3.9±0.2	None	—	—
J1023+4230	0.191	261±16	267	6.1±1.9	8.5±1.1	4.2±0.8	4.0±0.2	4.1±0.2	MaxBCGJ155.91525+42.48492	0.184	1.70
J1029+0420	0.105	228±12	209	2.6±0.8	8.5±1.1	3.0±0.7	4.3±0.3	4.1±0.2	None	—	—
J1032+5322	0.133	330±17	250	11.0±3.5	10.6±1.3	9.7±1.2	5.7±0.3	4.4±0.3	MaxBCGJ158.03906+53.32018	0.138	5.20
J1100+5329	0.317	—	303	3.5±1.1	6.3±0.6	3.1±0.7	1.9±0.1	4.1±0.2	None	—	—
J1103+5322	0.158	211±13	217	3.9±1.2	7.5±0.7	3.0±0.7	4.0±0.2	4.7±0.2	None	—	—
J1106+5228	0.095	283±14	239	2.1±0.7	10.8±2.0	1.7±0.5	3.5±0.2	4.9±0.5	NSCSJ110634+522247	—	6.10
J1112+0826	0.273	348±22	314	4.1±1.3	8.3±1.4	2.2±0.6	3.1±0.1	3.8±0.2	None	—	—
J1134+6027	0.153	257±13	242	6.6±2.1	11.9±1.8	4.4±0.8	4.2±0.2	5.1±0.3	None	—	—
J1142+1001	0.222	238±24	254	2.6±0.8	8.5±1.0	1.4±0.5	3.6±0.2	4.5±0.2	None	—	—
J1143-0144	0.106	279±13	285	237±75	12.5±1.6	11.2±1.3	3.0±0.2	4.7±0.5	SDSS-C41035	0.106	0.90
									ABELL1364	0.106	2.70
									MaxBCGJ176.02643-01.79024	0.257	9.60
J1153+4612	0.180	248±16	220	3.4±1.1	8.3±0.9	3.4±0.7	5.2±0.2	4.7±0.3	None	—	—
J1204+0358	0.164	290±18	254	37±12	8.8±1.4	15.9±1.6	4.7±0.2	4.3±0.3	MaxBCGJ181.14640+03.95642	0.165	2.30
									NSCJ120432+035012	0.116	8.40
									MaxBCGJ181.20101+03.98553	0.265	1.50
									ABELL1463	—	1.90
J1205+4910	0.215	299±15	285	2.3±0.7	7.2±1.1	2.2±0.6	2.8±0.1	3.6±0.2	None	—	—
J1213+6708	0.123	308±16	251	1.5±0.5	8.6±0.9	1.4±0.5	3.1±0.2	3.6±0.2	None	—	—
J1218+0830	0.135	231±12	254	1.4±0.4	9.2±1.2	1.2±0.4	3.2±0.2	4.5±0.2	None	—	—
J1250+0523	0.232	272±15	244	3.1±1.0	7.0±0.6	2.8±0.7	2.8±0.1	3.9±0.2	None	—	—
J1250-0135	0.087	260±13	—	5.8±1.8	12.4±2.2	6.7±1.0	3.1±0.2	4.5±0.4	None	—	—
J1251-0208	0.224	—	209	7.8±2.5	9.4±1.2	3.1±0.7	4.1±0.2	4.3±0.2	NSCJ125151-021711	0.169	10.00
J1259+6134	0.233	273±17	—	2.3±0.7	9.4±1.2	1.9±0.5	3.2±0.1	4.3±0.2	None	—	—
J1402+6321	0.205	283±18	294	1.8±0.6	9.8±1.1	1.7±0.5	2.7±0.2	4.3±0.3	NSCSJ140131+632201	0.350	6.40
J1403+0006	0.189	232±18	225	31.1±9.8	8.6±1.0	10.6±1.3	4.6±0.2	4.6±0.3	SDSSCEJ210.802505+00.093432	0.183	4.40
									MaxBCGJ210.85765+00.13363	0.167	1.60
J1416+5136	0.299	261±27	287	3.9±1.2	7.2±0.9	3.4±0.7	3.4±0.1	3.8±0.2	None	—	—
J1420+6019	0.063	220±11	204	1.8±0.6	10.4±1.4	1.7±0.5	5.1±0.4	5.4±0.4	None	—	—
J1430+4105	0.285	343±34	337	3.3±1.1	9.6±1.2	2.2±0.6	1.8±0.1	4.0±0.3	MaxBCGJ217.49493+41.10435	0.270	1.00
J1432+6317	0.123	205±10	236	—	—	—	—	—	None	—	—
J1436-0000	0.285	240±18	256	5.6±1.8	6.3±0.6	4.4±0.8	2.9±0.1	3.4±0.2	SDSSCEJ219.075027+00.094154	0.288	6.60
									SDSSCEJ218.997833-00.116972	0.139	9.60
J1443+0304	0.134	231±12	207	4.9±1.5	6.7±0.7	4.8±0.9	5.9±0.3	4.4±0.3	None	—	—
J1451-0239	0.125	238±15	222	3.8±1.2	7.8±0.8	3.9±0.8	3.6±0.2	4.4±0.3	ZwCl1449.1-0227	—	3.40
J1525+3327	0.358	279±28	318	1.2±0.4	8.3±1.0	1.1±0.4	1.9±0.1	4.3±0.2	NSCJ152503+332621	0.219	1.60
J1531-0105	0.160	297±15	281	4.8±1.5	8.9±0.8	4.4±0.8	3.4±0.2	4.5±0.2	SDSSCEJ232.866760-01.117970	0.129	5.70
									SDSSCEJ233.054077-01.151869	0.424	6.60
J1538+5817	0.143	205±13	222	7.9±2.5	8.9±1.1	2.8±0.7	4.8±0.2	4.8±0.3	None	—	—
J1618+4353	0.199	—	—	6.0±1.9	10.3±1.3	3.7±0.8	4.1±0.2	4.1±0.2	None	—	—
J1621+3931	0.245	253±21	285	2.3±0.7	7.8±0.9	2.3±0.6	2.6±0.1	4.1±0.2	None	—	—
J1627-0053	0.208	312±16	274	—	—	—	—	—	None	—	—
J1630+4520	0.248	297±17	311	2.0±0.6	9.8±1.1	1.7±0.5	2.8±0.1	4.2±0.2	None	—	—
J1636+4707	0.228	250±16	247	10.0±3.2	7.8±1.3	3.9±0.8	3.9±0.1	4.0±0.3	MaxBCGJ249.00650+47.11864	0.235	0.40
J1718+6424	0.090	—	—	10.0±3.2	10.5±2.0	4.1±0.8	3.6±0.2	4.2±0.3	SDSS-C43010	0.087	0.70
									NSCJ171819+642403	0.118	2.10
J2141-0001	0.138	195±15	—	2.6±0.8	7.8±0.9	2.3±0.6	5.2±0.3	4.1±0.2	None	—	—



TABLE 1 — *Continued*

Lens (1)	$z_l$ (2)	$\sigma_*$ (3)	$\sigma_{\text{SIE}}$ (4)	$\Sigma_{10}$ (5)	$\langle \Sigma_{10} \rangle_t$ (6)	$D_1$ (7)	$\langle D_1 \rangle$ (8)	$\langle D_1 \rangle_t$ (9)	Cluster Name (10)	$z_{cl}$ (11)	Dist (12)
J2238-0754	0.137	211±12	238	1.6±0.5	7.0±0.6	1.6±0.5	4.1±0.2	4.6±0.2	None	—	—
J2300+0022	0.228	301±18	301	—	—	—	—	—	None	—	—
J2302-0840	0.090	253±13	—	3.4±1.1	10.1±2.1	3.6±0.7	5.9±0.4	4.4±0.3	MaxBCGJ345.47648-08.74353	0.211	7.40
J2303+1422	0.155	269±17	290	4.5±1.4	8.7±1.0	3.4±0.7	3.7±0.2	4.3±0.3	MaxBCGJ345.79257+14.36653	0.159	2.80
J2321-0939	0.082	260±13	259	2.0±0.6	15.0±2.9	2.0±0.6	2.7±0.2	5.7±0.6	None	—	—
J2341+0000	0.186	218±14	262	9.9±3.1	8.4±1.2	5.1±0.9	3.1±0.2	4.6±0.3	SDSSCEJ355.279785-00.000869	0.197	1.20
									SDSSCEJ355.248779+00.081260	0.220	5.50
									NSCSJ234103+000250	0.110	3.30
									ABELL2644	0.069	5.30

NOTE. — Col. (1): Lens ID. Col. (2): Lens redshift. Col. (3): Central stellar velocity dispersion in  $\text{km s}^{-1}$ , when available. From paper V. Col. (4): Velocity dispersion of the best fit SIE model in  $\text{km s}^{-1}$ , when available. from Paper V. Col. (5): Surface density measured within the tenth nearest neighbor, in  $\text{Mpc}^{-2}$ . Col. (6): Average  $\Sigma_{10}$  for twins, in  $\text{Mpc}^{-2}$ . Col. (7): Surface density of neighbors within  $1h^{-1}\text{Mpc}$  radius, in  $\text{Mpc}^{-2}$ . Col. (8): Average  $D_1$  for random lines of sight, in  $\text{Mpc}^{-2}$ . Equal to average  $\Sigma_{10}$  for random lines of sight. Col. (9): Average  $D_1$  for twins, in  $\text{Mpc}^{-2}$ . Col. (10): Name of the clusters known to NED, within  $10'$ . Catalog references: *SDSSCE* Goto et al. (2002); *ZwCl* Zwicky et al. (1961); *MaxBCG* Koester et al. (2007); *NSC* Lopes et al. (2004); *Abell* Abell et al. (1989); *SDSS-C4* Miller et al. (2005). Col. (11): Redshift of the known cluster. Photometric redshifts are listed when spectroscopic redshifts are not available. Col. (12): Angular distance to the known cluster in arcminutes.